A Fundamental Investigation on Welding Flux Tunability Geared Towards High Heat Input Submerged Arc Welding for Shipbuilding Applications

H. Yuan[1], H. Tian[2], Y. Zhang[3], Z. Wang[4], and C. Wang[5]*

1. Ph.D. Candidate, School of Metallurgy, Northeastern University, Shenyang 110819, China. yuanhangneu@foxmail.com
2. Ph.D. Candidate, School of Metallurgy, Northeastern University, Shenyang 110819, China. tianhuiyu@omgmail.cn
3. Postdoctoral Researcher, School of Metallurgy, Northeastern University, Shenyang 110819, China. yanyun_zhang@foxmail.com
4. Associate Professor, School of Metallurgy, Northeastern University, Shenyang 110819, China. wangzhanjun@smm.neu.edu.cn
5. Professor, FASM, School of Metallurgy, Northeastern University, Shenyang 110819, China. wangc@smm.neu.edu.cn

Keywords: welding flux, element transfer, structure, physicochemical property

ABSTRACT

Submerged arc welding (SAW) is one of the significant metal-joining processes for manufacturing marine vessels, steel pipes, and offshore structures with high deposition rate and engineering reliability. Welding flux serves several essential functions, including atmospheric shielding, arc stabilization, bead morphology control, and weld metal (WM) refinement. Therefore, from a thermodynamic point of view, the focus for flux design and WM compositional/microstructural modification has been placed to elucidating the transfer pathways and mechanisms of major alloying elements, such as Si, Mn, Ti, and O during welding. To this end, a thermodynamic model has been established to predict alloying element contents in the WM. Such functions are enabled by the physicochemical properties of the fluxes, which are inherently rooted in the nature of the fluxes. A unique yet systematical investigation, including physicochemical property changes and structural evolution behaviours, has been conducted over the wide range of fluxes applied to actual welding of EH36 shipbuilding steels. Combined with spectroscopic methods, structural behaviours of network formers such as SiO_2, Al_2O_3, and TiO_2 and network modifiers such as MgO, MnO, and CaO have been illustrated. Viscosity and ionic conductivity have been found to be positively associated with the degree of polymerisation.

INTRODUCTION

High heat input submerged arc welding (SAW) technology, known for high deposition efficiency and excellent weld metal formability, has found widespread applications in various engineering fields (Yuan, Wang, Zhang and Wang, 2023). However, high heat input could produce coarse yet brittle microstructural constituents in the weld metal (WM), thus deteriorating mechanical properties of the entire weldment (Wu, Yuan, Kaldre, Zhong, et al., 2023). During SAW, various redox reactions and heat transfer events could occur in the arc cavity, in which fluxes could play significant roles in forming atmospheric shielding, refining WM, and preventing heat loss (Wang and Zhang, 2021). Such needed functions are enabled by appropriate flux thermophysical properties, such as viscosity and thermal conductivity (Zhang, Wang, Zhang, Li, et al., 2022). It is well known that thermophysical properties are structure dependent and largely dictated by the extent of chemical and topological disorder in the molten state (Wang, Li, Zhong, Li, et al., 2023). Therefore, a clear yet comprehensive understanding of flux structures is crucial to optimized design and enhanced welding performance. However, the current flux design mainly relies on empirical methods, lacking a comprehensive and systematic exploration of the flux structure and physicochemical properties. This deficiency leads to an ambiguous evolution of the flux structure-physicochemical properties.

Furthermore, fluxes should improve their metallurgical properties aside from satisfying the welding process. The WM mechanical properties under high heat input welding can be improved by fine-tuning the flux composition to precisely optimise the metallurgical properties. Specifically, the flux composition contributes significantly to the WM chemistry through chemical reactions occurring in the welding process (Zhang, Zhang, Liu, Wang, et al., 2022). For example, Zhang et al. (Zhang, Leng and Wang, 2019) designed TiO_2-containing basic-fluoride-type fluxes, enabling the transfer of Ti, Mn, and Si to the WM. They emphasized that optimal mechanical properties were achieved with the addition of 6 wt per cent TiO_2 in the flux. Therefore, addressing the roles of fluxes in regulating WM composition becomes urgent, as they are directly linked to the element transfer behaviours between the flux and WM.

This study aims to concentrate on the microstructure and physicochemical properties of flux modification. This work will gain an in-depth understanding of the flux characteristics and help to determine the guidelines for flux design in high heat input welding.

EXPERIMENTAL

All the experimental samples for the present welding fluxes were prepared from the reagent-grade powders of SiO_2, Al_2O_3, TiO_2, MnO, MgO, and CaO. The samples were thoroughly mixed and placed inside a pure molybdenum crucible, and were then pre-melted in the high-temperature region of the resistance furnace at 1550 °C under a pure argon atmosphere (>99.999 per cent, 0.3L/min). After being held at that temperature for 1 hour, the molten slags were quenched in cold water rapidly and then dried at 200 °C for 4 hours to remove any moisture. The as-quenched samples were crushed and ground into powders of less than 200 mesh. Viscosity measurements were carried out using the

rotating cylinder method with Brookfield viscometer, where one molybdenum crucible filled with 150 g flux sample was placed in an electric resistance furnace.

Structural information was identified through spectroscopic analyses using Raman spectroscopy and X-ray photoelectron spectroscopy (XPS). Raman was carried out by a laser confocal Raman spectrometer (LabRam HR800, Horiba, United States) with a 1-mW semiconductor laser using a 532 nm excitation wavelength. The spectra were recorded with a 1 cm^{-1} resolution ranging from 400 to 1600 cm^{-1}. At least ten spectra were acquired for each sample to increase the reliability of the measures. XPS analysis was performed using an imaging photoelectron spectrometer (Thermo Scientific K-Alpha, United States) at room temperature with a monochromatic Al-Kα X-ray source with a pass energy of 50 eV. The spectra were calibrated by taking the C 1s peak as the reference binding energy at 284.8 eV.

Double-wire SAW was performed on the base metal of EH36 shipbuilding steel. Welding parameters (electrode forward: DC-850 A/32 V, electrode backward: AC-625 A/36 V) were kept constant with the travel speed at 500 mm/min.

RESULTS AND DISCUSSIONS

Transfer behaviours of Si, Mn, Ti, and O

The element transfer between slag and WM is quantified by a Δ value and refers to the difference between analytical composition and nominal composition of the WM (Zhang, Wang and Coetsee, 2021). The Δ value indicates the contribution of flux to the WM composition. A positive Δ value implies that a specific element has been transferred from flux(slag) to WM. A negative Δ value means that a given element has been lost from WM to slag. For a specific element, a zero Δ value implies that an apparent equilibrium condition has been reached between the slag and WM (Zhang, Coetsee, Dong and Wang, 2020).

In the droplet zone of the SAW, where droplet forms at the electrode tip and travels through the arc, most oxides are susceptible to decompose and thus increase the O level of the droplet by increasing the local p_{O2} via Reactions (1) and (2) under the presence of the arc. In this period, O level of the droplet increases, and negligible amount of alloy transfer, such as Si and Mn, may occur.

$$(MnO)=Mn(g)+1/2O_2(g) \quad (1)$$

$$(SiO_2)=SiO(g)+1/2O_2(g) \quad (2)$$

Subsequently, the droplet is diluted by the weld pool, and the transfer of Mn and O at slag-metal interface would be governed by Reaction (3).

$$(MnO)=[Mn]+[O] \quad (3)$$

Table 1 summarizes the Δ values of the WMs. As can be seen from Table 1, the ‘neutral point’ of Mn for WMs, where equilibrium is built between slag and WM apparently, lies at between 10~20 wt per cent MnO. For Flux with MnO addition of 0 and 10 wt per cent, the WMs lose 0.318 and 0.162 wt per cent Mn to the slags, respectively; for the MnO-rich fluxes, the WMs gain up to 0.588 wt per cent Mn from the slags. All WMs gain Si from the slags with an average value of about 0.187 wt per cent. The transfer of Si appears to be independent of MnO content in the fluxes.

Flux plays a major role in O uptake of the WM in SAW (Zhang, Liu, Coetsee, Wang, et al., 2023). MnO and SiO_2 are reported as primary sources of O in SAW. It is observed from Table 1 that there is a significant increase in ΔO values from 150 to 850 ppm as MnO content increases from 0 to 60 wt per cent. In the droplet zone, O is transferred to the droplet via the increase of p_{O2} in Reactions (1) and (2) as mentioned previously. It is deduced from Reaction (1) that p_{O2} would increase with higher MnO content in the fluxes for a given amount of SiO_2. In the weld pool zone, the transfer of O to the WM increases with MnO addition as Reaction (3) is promoted to the right side.

Although the transfer mechanism of O from CaO to WM remains ambiguous, it is accepted that CaO is one of the most stable oxides with a lower O potential than MnO. The amount of O contributed from the flux, viz. ΔO value, increases from 576 to 920 ppm at higher MnO content. It is seen that the ΔSi value generally increases with higher MnO additions in the flux. The addition of MnO tends to increase the activity of SiO_2, which, in turn, promotes the transfer of Si from flux to the weld metal.

Only a slight improvement of measured ΔMn value from 0.218 to 0.377 wt per cent is observed, although the MnO addition level dramatically increases from 10 to 60 wt per cent. This can be attributed to the fact that the evaporation of Mn from the weld pool tends to occur at the plasma-metal interface, reducing the magnitude of ΔMn value.

TABLE 1 – Changes of chemical compositions of WMs (Weight Percent)

CaF_2-40%SiO_2-MnO				CaO-40%SiO_2-MnO				25%CaF_2-SiO_2-CaO-TiO_2		
MnO	ΔSi	ΔMn	ΔO	MnO	ΔSi	ΔMn	ΔO	TiO_2	ΔTi	ΔO
0	0.212	-0.318	0.015	10	0.081	0.218	0.058	0	-0.002	0.018
10	0.193	-0.162	0.033	20	0.071	0.244	0.061	5	0.002	0.021
20	0.164	0.125	0.038	30	0.082	0.278	0.069	10	0.005	0.023
30	0.16	0.092	0.045	40	0.118	0.344	0.084	15	0.007	0.025
40	0.163	0.318	0.058	50	0.167	0.327	0.092	20	0.01	0.027
50	0.216	0.437	0.085	60	0.16	0.377	0.085			
60	0.201	0.588	0.08							

Gas–slag–metal model

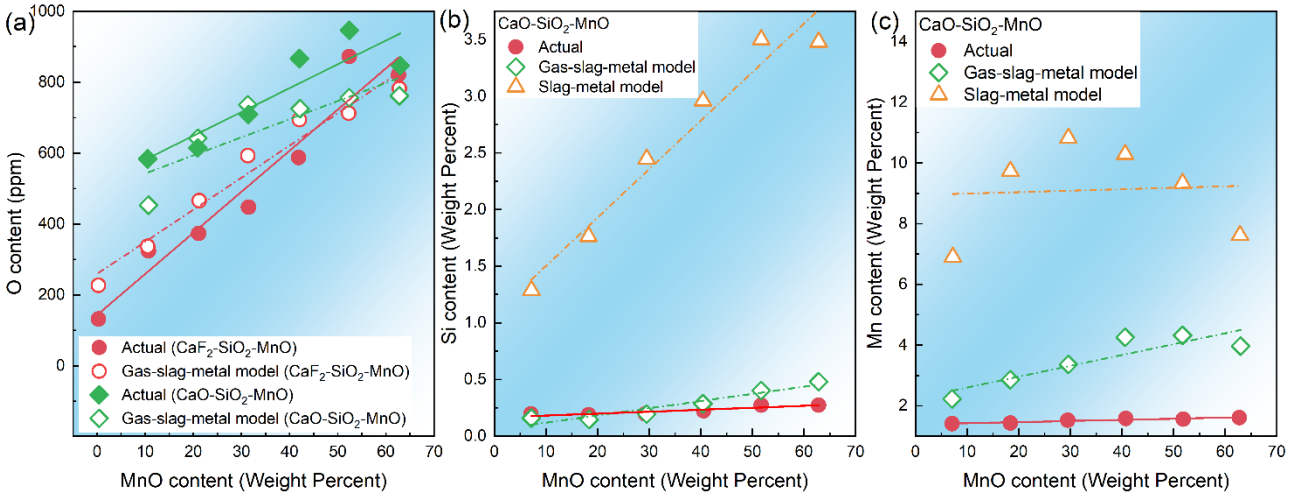

FIG 1 –Predicted contents by gas–slag–metal equilibrium calculations for (a) O, (b) Si and (c) Mn content as a function of MnO level in fluxes.

Results above have quantified the element transfer behaviours. Therefore, to precisely predict the essential element contents, a gas–slag–metal equilibrium model is established, based on the assumption that the the O level is controlled by p_{O2} (derived from the decomposition of the oxide in flux) in the arc plasma. Figure 1 shows the predicted contents by gas–slag–metal equilibrium calculations for Si, Mn, and O. It can be seen that this model offers excellent prediction accuracy for O content, and can differentiate the O content of the weld metals produced by fluxes with varying formulas but same basicity index. Furthermore, when the gas–slag–metal equilibrium model is applied, the prediction error for Si and Mn contents is significantly reduced as compared to the slag–metal equilibrium model. Thermodynamic calculation data indicates that the consideration of gas formation, which essentially controls the predicted flux O potential and oxide activity, is necessary to improve the overall prediction accuracy.

Transfer pathway of oxygen

It is revealed that O transfer behaviour could likely be a dynamic process involving O gain and loss. A practical challenge is that the dynamic process is covered under molten flux, which is difficult to observe and quantify directly. O transfer processes are related to O transfer pathways that can be deciphered by WM O gain and loss. However, controversies remain regarding the transfer pathway

for O, which dims the understanding of the O transfer mechanism. Hence, further investigations are called upon to account for the transfer pathway of O in pertinent welding fluxes.

At the slag–metal reaction interface, the transfer of O is largely enabled simultaneously with the transfer of other alloying elements via Reactions (4) and (5) in CaF_2-SiO_2-CaO-(0~20 wt per cent)TiO_2 system. Table 2 shows the WM O gain by slag–metal reactions. O contributions from SiO_2 and TiO_2 are denoted as ΔO_{SiO2} and ΔO_{TiO2}, respectively. It is seen that positive ΔO_{SiO2} and ΔO_{TiO2} values increase with higher TiO_2 content in the flux, indicating O transfer from the flux to the WM. WM O gain is favoured with enhanced TiO_2 content, which will increase the activities of SiO_2 and TiO_2. What stands out is that, for any given TiO_2 content, ΔO_{SiO2} value is over ten times that of ΔO_{TiO2}, which could be attributed to the fact that the O potential of SiO_2 is reportedly higher than that of TiO_2 during the welding process, as manifested by the high WM O levels for multi-component acidic fluxes with high SiO_2 contents. Moreover, Table 2 also shows actual changes of the O content in the WM. Total O gain of the WM through slag–metal reactions increases from 0.267 to 0.389 wt per cent. However, actual WM ΔO ranges from 0.018 to 0.027 wt per cent, suggesting that there is O loss in the WM after WM gains O by slag–metal reactions.

$$(TiO_2)=[Ti]+2[O] \quad (4)$$

$$(SiO_2)=[Si]+2[O] \quad (5)$$

O loss incurred by Fe, Mn, and C is denoted as ΔO_{Fe}, ΔO_{Mn}, and ΔO_C. It is demonstrated that ΔO_{Fe}, ΔO_{Mn}, and ΔO_C are always negative, and their absolute values increase with higher TiO_2 content, indicating O loss from the WM to the slag. O loss by oxidation of Fe from the WM increases from 0.23 to 0.31 wt per cent, which is significantly larger than those of ΔO_{Mn} and ΔO_C, suggesting that deoxidation of the WM is mainly attributed to oxidation of Fe. In addition, the WM O content reduced by deoxidation is 0.268 to 0.389 wt per cent with TiO_2 increase from 0 to 20 wt per cent, which is greater than that of the O gain (0.267 to 0.355 wt per cent) by slag–metal reactions, indicating another pathway for the WM to gain O is through gas–metal reactions. It is concluded that gas–metal reactions mainly occur in the ‘‘droplet zone’’, the region where droplets form at the electrode tip and travel through the arc cavity. Wt conservation calculations of WM can be used to calculate O gain (ΔO_{gas}) through gas–metal reactions, which can be calculated by Equation (6). ΔO_{gas} content picks up from 0.017 to 0.062 wt per cent as TiO_2 content in the flux increases from 0 to 20 wt per cent.

$$\Delta O_{WM}=(\Delta O_{SiO2}+\Delta O_{TiO2}+\Delta O_{gas})-(\Delta O_{FeO}+\Delta O_{MnO}+\Delta O_{CO}) \quad (6)$$

WM O gain is primarily driven by gas–slag–metal reactions, while O loss is largely enabled by slag–metal reactions. The total O gain and loss increase from 0.286 to 0.416 and 0.268 to 0.389 wt per cent, respectively, and WM O gain is greater than its loss. This result indicates a net O gain (Total O gain minus total O loss, 0.018 to 0.027 wt per cent) in the WM, resulting in increased WM O content compared to the BM or electrode. Moreover, ΔO_{SiO2} contributes above 80 per cent to the total O gain, indicating that SiO_2 in the flux is the main O source for the WM. Fe deoxidation is the largest contributor to the WM O loss, demonstrated by ΔO_{Fe}, which accounts for more than 80 per cent of the total O loss.

TABLE 2 – Weld metal ΔO content as a function of TiO_2 content in the flux. (Weight Percent)

TiO_2(%)	**ΔO**	**Gain O**			**Loss O**		
		ΔSiO_2	ΔTiO_2	gas	C	Mn	Fe
0	0.018	0.269	0	0.003	-0.008	-0.029	-0.217
5	0.021	0.272	0.004	0.018	-0.01	-0.033	-0.23
10	0.023	0.288	0.007	0.036	-0.014	-0.04	-0.254
15	0.025	0.313	0.012	0.045	-0.014	-0.054	-0.277
20	0.027	0.338	0.017	0.053	-0.018	-0.057	-0.306

It can be concluded that oxides dissociate under the high temperature of the arc plasma, and O generated by TiO_2 and SiO_2 dissolves into the electrode droplets and WM. O generated by TiO_2 and SiO_2 dissolves into the electrode droplets and WM by gas–metal reactions, which accounts for 5.91 to 14.68 per cent of the total O gain. In addition, O also transfers from the molten flux into the WM

through Reactions (4) and (5), and SiO_2 in the flux is the most significant contributor to the O gain for the WM, accounting for more than 80 per cent of the total O gain. The solubility of O in WM decreases after the molten welding pool cools down from higher temperature to the solidification temperature. Therefore, Fe, Mn, and C will react with dissolved O, and then the deoxidation products will transfer into the slags. Oxidation of Fe is the main way for O loss from the WM, which has been demonstrated by ΔO_{Fe} accounts for more than 80 per cent of the total O loss.

Structure and physicochemical properties

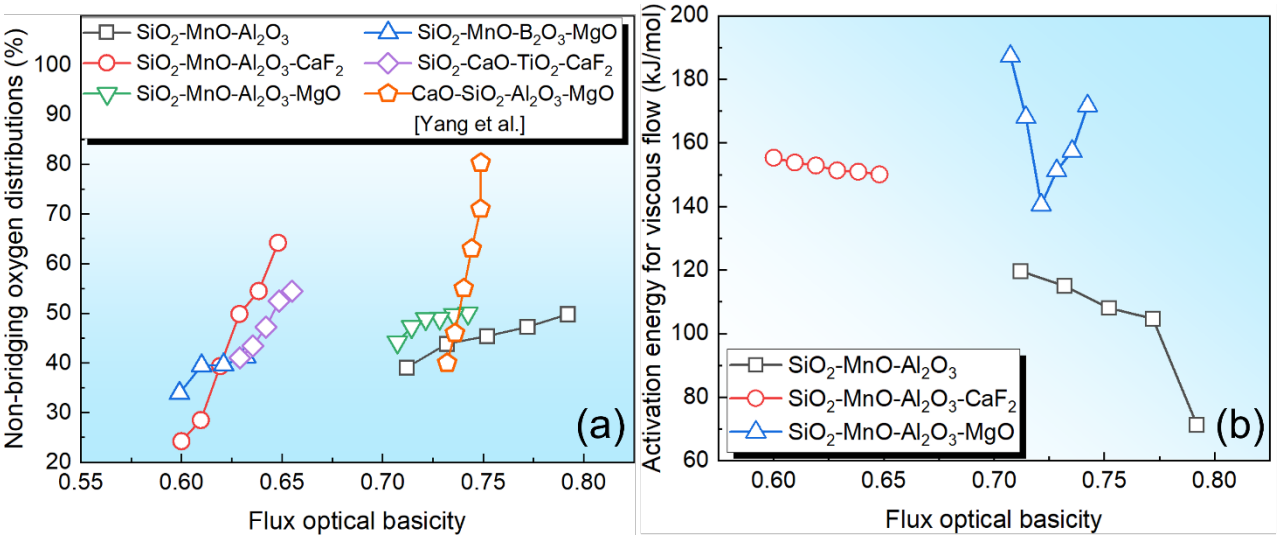

FIG 2 – Relationship between flux optical basicity and (a) non-bridging oxygen, and (b) activation energy for viscous flow.

The optical basicity (Λ) is a measure of the electron donor properties of different ions (Mills, Yuan and Jones, 2011, Mills, Yuan, Li, Zhang, et al., 2012). It was also used as a theoretical measure of the depolymerisation of the melt. In terms of experiment methods, XPS analysis possesses a unique function by showcasing features of various oxygen species, including O^-(non-bridging oxygen), O^0(bridging oxygen) and O^{2-} (free oxygen), which are closely related to the degree of polymerization of the flux structure (Wang, Shen, Zhong, Li, et al., 2023, Zhang, Coetsee, Yang, Zhao, et al., 2020). Therefore, the non-bridging oxygen distributions as a function of optical basicity for varied flux systems are shown in Figure 2a. It can be seen that the fraction of non-bridging oxygen increases with an increase in optical basicity for all the fluxes, which is consistent with earlier study (Yang, Wang and Sohn, 2022).

The activation energy (E_a) represents the frictional resistance within the structural units of the liquid flux that needs to be overcome during shearing (Wang, Zhang, Zhong and Wang, 2022). For Newtonian fluids, E_a can be obtained from the Arrhenius equation, as shown in Equation (7),

$$\ln\eta=\ln\eta_0+(E_a)/R\cdot 1/T \quad (7)$$

where η is the viscosity (Pa s), η_0 is a pre-exponential factor (Pa s), E_a is the activation energy for viscous flow (J/mol), T is the absolute temperature (K), and R is the ideal gas constant (8.314 J mol^{-1} K^{-1}). The calculated E_a values with different Al_2O_3 contents are shown in Figure 2b. As can be seen, E_a gradually decreases as the optical basicity increases. However, for the SiO_2-MnO-Al_2O_3-CaF_2 system, E_a decreases from 171.68 to 140.53 kJ mol^{-1} as the Al_2O_3 content increases from 0 to 15 wt per cent and then E_a shows a significant increase from 168.05 to 187.26 kJ mol^{-1} with further addition of Al_2O_3, which correlates well with the ‘‘V’’-shaped variation trend of the viscosity.

CONCLUSIONS

In summary, the transfer pathways and mechanisms of major alloying elements, such as Si, Mn, Ti, and O during welding have been elucidated. A thermodynamic model has been established to predict alloying element contents in the WM. Combined with spectroscopic methods, the flux optical basicity has been found to be positively associated with the degree of polymerisation. Moreover, the activation energy for viscous flow gradually decreases as the optical basicity increases.

ACKNOWLEDGEMENTS

The authors sincerely thank the National Natural Science Foundation of China (Grant Nos. U20A20277 and 52350610266) and National Key Research and Development Program of China (Grant No. 2022YFE0123300).

REFERENCES

Mills, K C, Yuan, L and Jones, R T, 2011. Estimating the physical properties of slags. *Journal of the Southern African Institute of Mining and Metallurgy* 111: 649-658.

Mills, K C, Yuan, L, Li, Z, Zhang, G H and Chou, K C, 2012. A review of the factors affecting the thermophysical properties of silicate slags. *High Temperature Materials and Processes* 31 (4-5): 301-321.

Wang, C and Zhang, J, 2021. Fine-tuning weld metal compositions via flux optimization in submerged arc welding: An overview. *Acta Metallurgica Sinica* 57 (9): 1126-1140.

Wang, Z, Li, Z, Zhong, M, Li, Z and Wang, C, 2023. Elucidating the effect of Al_2O_3/SiO_2 mass ratio upon SiO_2-MnO-CaF_2-Al_2O_3-based welding fluxes: Structural analysis and thermodynamic evaluation. *Journal of Non-Crystalline Solids* 601: 122071.

Wang, Z, Shen, B, Zhong, M, Li, Z and Wang, C, 2023. A structure-oriented elucidation for viscous flow of SiO_2-MnO-Al_2O_3 fused submerged arc welding fluxes. *Journal of Non-Crystalline Solids* 612: 122360.

Wang, Z, Zhang, J, Zhong, M and Wang, C, 2022. Insight into the viscosity–structure relationship of MnO–SiO_2–MgO–Al_2O_3 fused submerged arc welding flux. *Metallurgical and Materials Transactions B* 53: 1364-1370.

Wu, Y, Yuan, X, Kaldre, I, Zhong, M, Wang, Z and Wang, C, 2023. TiO_2-Assisted microstructural variations in the weld metal of EH36 shipbuilding steel subject to high heat input submerged arc welding. *Metallurgical and Materials Transactions B* 54 (1): 50-55.

Yang, J, Wang, Z and Sohn, I, 2022. Topological understanding of thermal conductivity in synthetic slag melts for energy recovery: An experimental and molecular dynamic simulation study. *Acta Materialia* 234: 118014.

Yuan, H, Wang, Z, Zhang, Y and Wang, C, 2023. Roles of MnO and MgO on structural and thermophysical properties of SiO_2-MnO-MgO-B_2O_3 welding fluxes: A molecular dynamics study. *Journal of Molecular Liquids* 386: 122501.

Zhang, J, Coetsee, T, Dong, H and Wang, C, 2020. Element transfer behaviors of fused CaF_2-SiO_2-MnO fluxes under high heat input submerged arc welding. *Metallurgical and Materials Transactions B* 51 (3): 885-890.

Zhang, J, Leng, J and Wang, C, 2019. Tuning weld metal mechanical responses via welding flux optimization of TiO_2 content: application into EH36 shipbuilding steel. *Metallurgical and Materials Transactions B* 50 (5): 2083-2087.

Zhang, J, Wang, C and Coetsee, T, 2021. Thermodynamic evaluation of element transfer behaviors for fused CaO-SiO_2-MnO fluxes subjected to high heat input submerged arc welding. *Metallurgical and Materials Transactions B* 52: 1937-1944.

Zhang, Y, Coetsee, T, Yang, H, Zhao, T and Wang, C, 2020. Structural roles of TiO_2 in CaF_2-SiO_2-CaO-TiO_2 submerged arc welding fluxes. *Metallurgical and Materials Transactions B* 51 (5): 1947-1952.

Zhang, Y, Liu, H, Coetsee, T, Wang, Z and Wang, C, 2023. Identifying oxygen transfer pathways during high heat input submerged arc welding: a case study into CaF_2-SiO_2-CaO-TiO_2 fluxes. *Metallurgical and Materials Transactions B* 54 (6): 2875-2880.

Zhang, Y, Wang, Z, Zhang, J, Li, Z, Basu, S and Wang, C, 2022. Probing viscosity and structural variations in CaF_2–SiO_2–MnO welding fluxes. *Metallurgical and Materials Transactions B* 53 (5): 2814-2823.

Zhang, Y, Zhang, J, Liu, H, Wang, Z and Wang, C, 2022. Addressing weld metal compositional variations in EH36 shipbuilding steel processed by CaF_2-SiO_2-CaO-TiO_2 fluxes. *Metallurgical and Materials Transactions B* 53: 1329-1334.